

Surface sensing triggers a broad-spectrum antimicrobial response in *Pseudomonas aeruginosa*

Bartosz Gerard Gdaniec ^{1,2}, Pierre-Marie Allard,³
Emerson Ferreira Queiroz,³ Jean-Luc Wolfender,³
Christian van Delden^{1,2} and Thilo Köhler ^{1,2*}

¹Transplant Infectious Diseases Unit, University Hospital Geneva, Geneva, Switzerland.

²Department of Microbiology and Molecular Medicine, University of Geneva, Geneva, Switzerland.

³School of Pharmaceutical Sciences, EPGL, University of Geneva, University of Lausanne, Geneva, Switzerland.

Summary

Interspecies bacterial competition may occur via cell-associated or secreted determinants and is key to successful niche colonization. We previously evolved *Pseudomonas aeruginosa* in the presence of *Staphylococcus aureus* and identified mutations in the Wsp surface-sensing signalling system. Surprisingly, a $\Delta wspF$ mutant, characterized by increased c-di-GMP levels and biofilm formation capacity, showed potent killing activity towards *S. aureus* in its culture supernatant. Here, we used an unbiased metabolomic analysis of culture supernatants to identify rhamnolipids, alkyl quinoline N-oxides and two siderophores as members of four chemical clusters, which were more abundant in the $\Delta wspF$ mutant supernatants. Killing activities were quorum-sensing controlled but independent of c-di-GMP levels. Based on the metabolomic analysis, we formulated a synthetic cocktail of four compounds, showing broad-spectrum anti-bacterial killing, including both Gram-positive and Gram-negative bacteria. The combination of quorum-sensing-controlled killing and Wsp-system mediated biofilm formation endows *P. aeruginosa* with capacities essential for niche establishment and host colonization.

Introduction

Whether in the environment or during host infection, bacteria have to compete with established microbial communities to gain access to nutrients and space. Typical examples for polymicrobial infections are burn wounds and cystic fibrosis (CF) lungs, where the dominant pathogenic species are *Pseudomonas aeruginosa* and *Staphylococcus aureus*. Although *S. aureus* is prevalent in young CF patients, *P. aeruginosa* occurs more frequently in adult respiratory samples (Folkesson *et al.*, 2012). This switch in colonization frequency might result from host immune responses, antibiotic treatments and/or from direct competition between the two microorganisms (Limoli and Hoffman, 2019). Focusing on the latter hypothesis, we have previously established an *in vitro* model in which we evolved *P. aeruginosa* for 150 generations in the presence and absence of *S. aureus* to assess how *P. aeruginosa* adapts to the presence of a pre-established niche competitor (Tognon *et al.*, 2017). By comparing the genomes of ancestor and evolved populations, we observed emergence of mutations in the *P. aeruginosa* Wsp (wrinkly spreader phenotype) signal transduction system (D'Argenio *et al.*, 2002; Hickman *et al.*, 2005). The mutations occurred in the *wspF* gene, resulting in constitutive activation of the Wsp signalling cascade. Surprisingly, the *wsp* mutants showed increased killing activity against *S. aureus* in comparison to the ancestor strain PA14.

The Wsp signal transduction system of *P. aeruginosa* is similar to the chemosensory system of *Escherichia coli* and uses methylation and demethylation of the WspA transmembrane sensor by WspE and WspF, respectively, to adapt to variations of external stimuli (D'Argenio *et al.*, 2002; Hickman *et al.*, 2005). The Wsp system in *P. aeruginosa* was reported to respond to surface attachment (Guvener and Harwood, 2007; O'Connor *et al.*, 2012; Song *et al.*, 2018) and to changes in membrane composition (Blanka *et al.*, 2015). These stimuli ultimately translate into the generation of the intracellular signalling molecule c-di-GMP, via the cognate di-guanylate cyclase WspR, entailing increased polysaccharide production, cell aggregation and biofilm formation (Kulasakara *et al.*, 2006; Valentini and Filloux, 2016). Loss of function mutations in the methyl esterase WspF results in constitutive activation

Received 27 April, 2020; revised 15 June, 2020; accepted 21 June, 2020. *For correspondence. E-mail thilo.kohler@unige.ch; Tel. +41 22 379 55 71; Fax +41 22 379 57 02.

of the Wsp signalling cascade and hence increased c-di-GMP levels (Hickman *et al.*, 2005). Compared to the wild type, *wspF* mutants are less motile and display a typical wrinkly colony morphology and reduced colony size, a phenotype reminiscent of the wrinkly spreaders described initially in *P. fluorescens* (Spiers *et al.*, 2002). The secondary messenger c-di-GMP plays a major role in the switch between the two main lifestyles of bacteria: the motile, planktonic lifestyle, associated with low c-di-GMP levels, and the sessile biofilm mode of growth triggered by high intracellular levels of c-di-GMP (Valentini and Filloux, 2016). *Wsp* mutants emerge *in vitro* upon exposure of *P. aeruginosa* to sub-lethal concentrations of hydrogen peroxide (Chua *et al.*, 2016), but also *in vivo* during chronic lung infection in CF patients and in burn wounds (Smith *et al.*, 2006; Starkey *et al.*, 2009; Marvig *et al.*, 2015; Gloag *et al.*, 2019).

The observation that *P. aeruginosa*, programmed for the sessile lifestyle, also displays antibacterial activity, prompted us to analyse the supernatants of a *wspF* mutant, using metabolomics analysis. We show that metabolite clusters comprising rhamnolipids, alkyl quinoline N-oxides and the siderophores pyochelin and pyoverdine are the most upregulated chemical species in the *wspF* supernatant compared to the ancestor PA14. We observed a coordinated antibacterial action of these compounds and were able to reconstitute an artificial cocktail showing a broad-spectrum antibacterial activity against Gram-positive and Gram-negative species. Hence, switching-on the Wsp signalling system during biofilm formation also protects against invading or established competitors.

Results

Metabolomic analysis reveals overproduction of rhamnolipids, siderophores and N-oxide quinolones in ΔwspF mutant supernatant

We have previously shown that a *P. aeruginosa* $\Delta wspF$ mutant supernatant presents killing activity against *S. aureus* (Tognon *et al.*, 2017). To identify secreted bacterial compounds in an unbiased and global approach, we profiled supernatants of the PA14 reference strain and a $\Delta wspF$ mutant by Ultra-High Performance Liquid Chromatography high-resolution tandem mass spectrometry (UHPLC-HR/MSMS). The HR/MSMS datasets were organized as a molecular network (MN), which provides tandem fragmentation spectra according to their spectral similarity (Wang *et al.*, 2016). The experimental fragmentation dataset in the MN was annotated by comparison with a database of simulated spectra of natural products obtained by *in silico* MS/MS fragmentation (Allard *et al.*, 2016) and following a taxonomically informed metabolite annotation process (Rutz *et al.*, 2019). In a MN, a cluster

of nodes is generally indicative of a family of structurally related molecules. We further integrated in the MN the relative intensities of all detected metabolites in the supernatants. We reasoned that compounds with potential killing activity were more abundant in supernatants of a $\Delta wspF$ mutant (red colour in nodes) than in those of the PA14 wild type strain (blue colour in nodes). Based on this assumption, we identified four distinct clusters belonging to alkyl quinoline N-oxides (AQNOs), rhamnolipids, pyoverdine and pyochelin families (Figs 1 and S1). The AQNO cluster was composed of several compounds showing variable distributions between the $\Delta wspF$ mutant and the PA14 wild type supernatants (Fig. 1A). Indeed, *P. aeruginosa* synthesizes more than 50 different alkyl-quinolones, sharing a common biosynthetic pathway with the *Pseudomonas* quinolone signal (PQS) (Lepine *et al.*, 2004; Drees *et al.*, 2018). Analysis of the AQNO sub-group identified four compounds: 2-heptyl-4-quinoline N-oxide (HQNO), 2-nonyl-4-quinoline N-oxide (NQNO), 2-decanoyl-4-quinoline N-oxide (DQNO) and 2-undecanoyl-4-quinoline N-oxide (UQNO). The metabolomic analysis detected similar amounts of HQNO and UQNO, but increased amounts of NQNO and DQNO in the $\Delta wspF$ mutant supernatants compared to those of PA14 (Fig. S2A), suggesting that these latter compounds might contribute to *S. aureus* killing.

A detailed analysis of the rhamnolipid cluster (cluster B in Fig. 1), almost exclusively detected in the $\Delta wspF$ mutant supernatants, revealed mainly the presence of C₁₀ and C₁₂ mono-rhamnolipids as well as C₁₀-C₁₀ and C₁₂-C₁₂ di-rhamnolipids, both being produced by the majority of *P. aeruginosa* isolates (Abdel-Mawgoud *et al.*, 2010). In agreement with the metabolomic data, the orcinol assay detected 11-fold higher amounts of rhamnolipids in a $\Delta wspF$ mutant supernatant compared to those of PA14 (Fig. S2B).

Pyoverdine and pyochelin, the main siderophores produced by *P. aeruginosa*, were members of two clusters, which were mainly detected in the $\Delta wspF$ mutant supernatants (Fig. 1, clusters C and D). Spectrophotometric quantification of the two siderophores confirmed the metabolomics data, showing a 30-fold increase in pyoverdine (Fig. S2C) and a twofold increase in pyochelin concentrations in $\Delta wspF$ mutant supernatants compared to those of PA14 (Fig. S2D).

Altogether, the metabolomics analysis detected members of three important classes of *P. aeruginosa* virulence factors, namely rhamnolipids, siderophores and two AQNOs, which were present in higher amounts in a $\Delta wspF$ supernatant compared to those of PA14.

Metabolites overexpressed in the ΔwspF mutant all contribute to S. aureus killing activity

To determine whether specific compounds identified by the metabolomics analyses were essential for the *S. aureus*

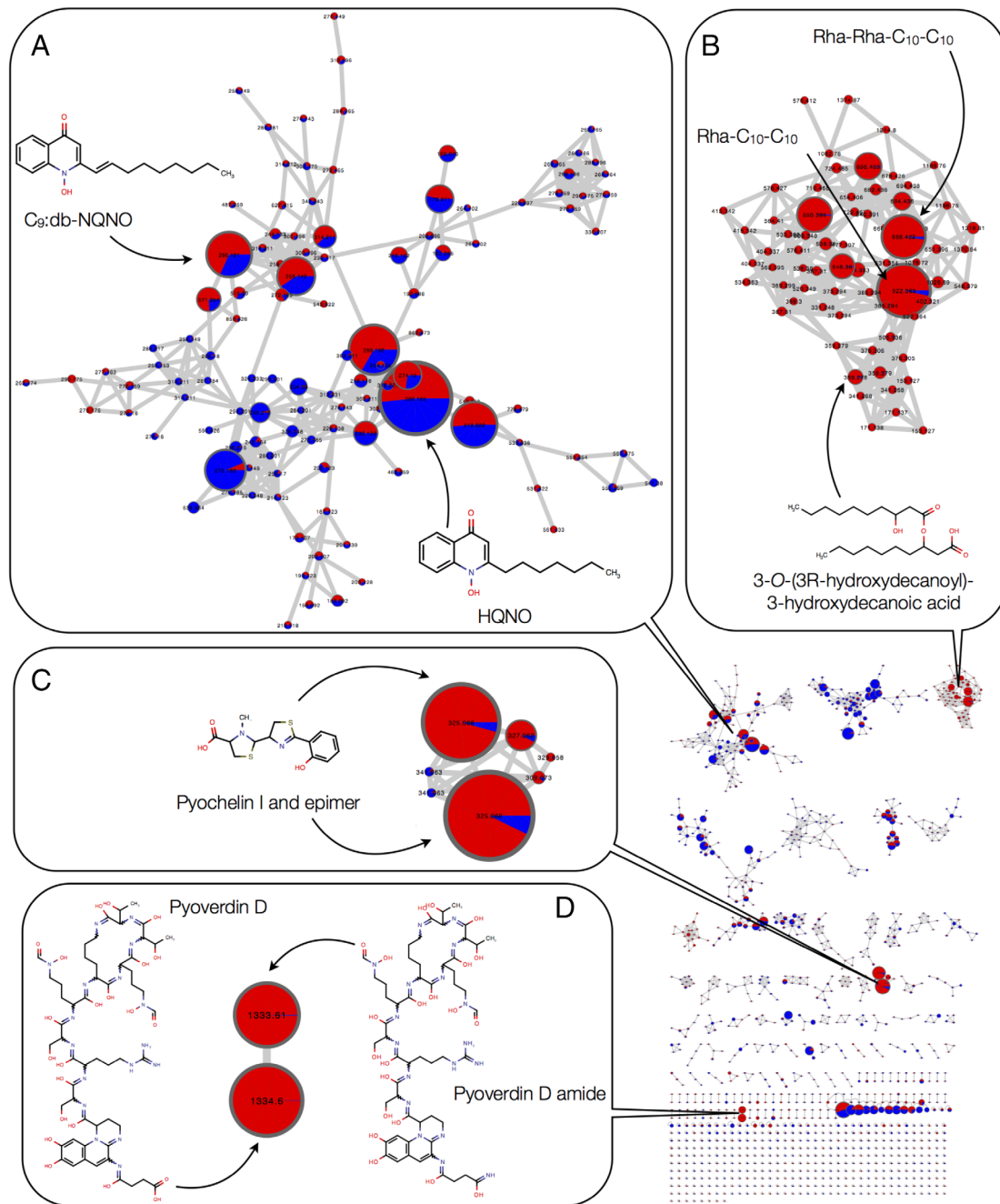


Fig 1. Metabolomic analysis and molecular networks of PA14 and $\Delta wspF$ supernatants. The molecular network is shown on the right. The identified compound families are represented as nodes (circles), showing their molecular masses in the node centres. The relative proportion of each compound family in supernatants of PA14 wild type and $\Delta wspF$ mutant are represented as blue and red coloured sections respectively. Nodes which show increased abundance in the $\Delta wspF$ mutant supernatants include the alkyl *N*-oxide quinoline cluster (A), the rhamnolipid cluster (B), the pyochelin (C) and pyoverdin clusters (D). [Color figure can be viewed at wileyonlinelibrary.com]

killing activity, we created deletion mutants in their corresponding biosynthetic pathways in a $\Delta wspF$ strain background (Table S1). Deletion of the *pchAD* operon, abolishing pyochelin synthesis, reduced the killing activity of the $\Delta wspF$ supernatant 10-fold. Simultaneous inactivation of the *pvdL* gene, involved in pyoverdin synthesis, further reduced the killing activity by three orders of

magnitude. Specific deletion of the *rhlA* gene, abolishing synthesis of all rhamnolipid species, decreased the killing activity by 3-logs, whereas deletion of the *pqsL* gene, encoding the *N*-oxide synthase responsible for AQNOs synthesis, reduced the *S. aureus* killing by 4-logs (Fig. 2A). We further measured HCN production, another secondary metabolite showing antimicrobial activity. HCN production

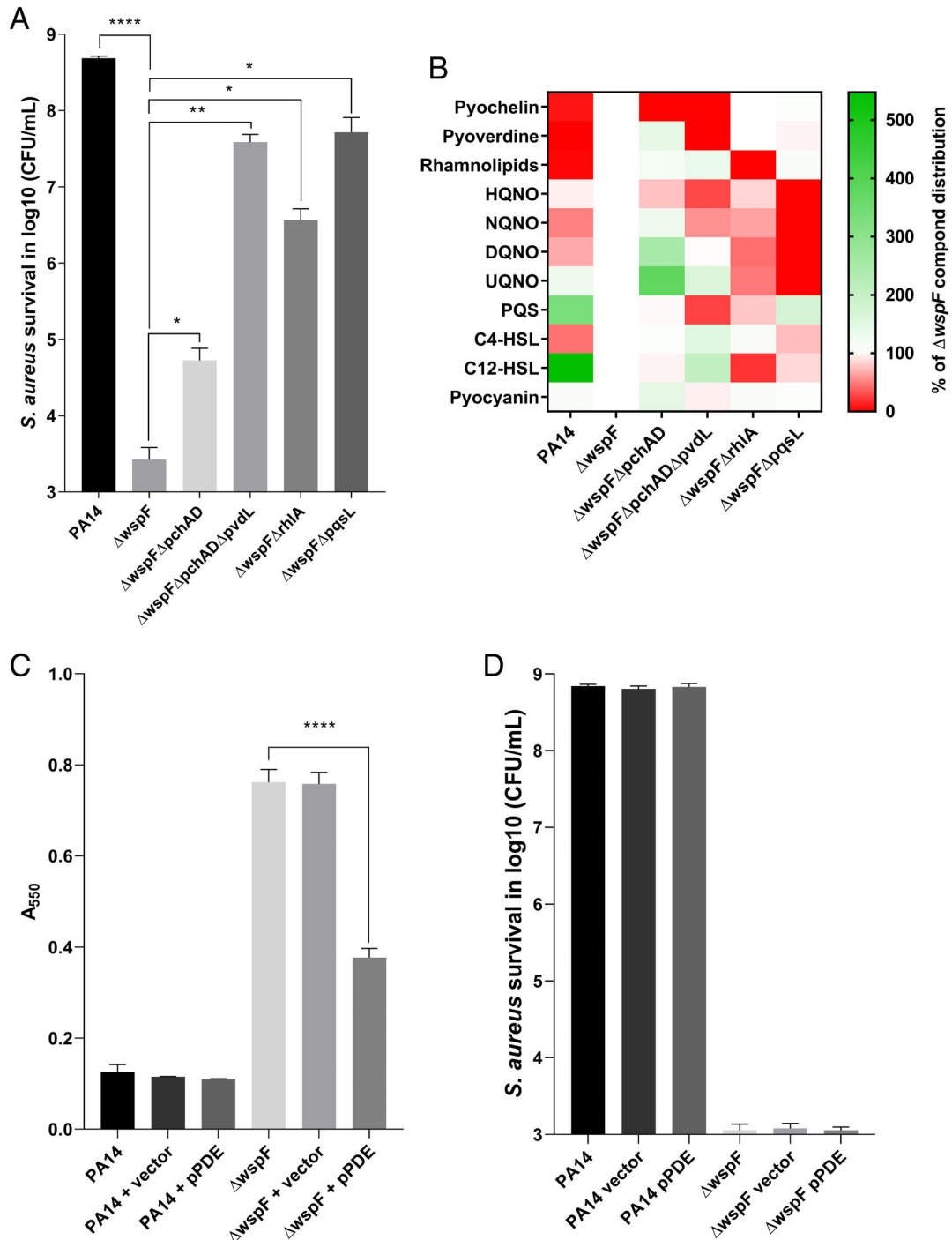


Fig 2. *S. aureus* killing activity of $\Delta wspF$ mutant is not dependent on c-di-GMP but involves QS-regulated metabolites.

A. Killing assay with supernatants of mutants deficient in production of pyochelin ($\Delta wspF\Delta pchAD$), pyochelin and pyoverdine ($\Delta wspF\Delta pchAD\Delta pvdL$), rhamnolipids ($\Delta wspF\Delta rhlA$) and N-oxide quinolines ($\Delta wspF\Delta pqsL$) were performed on *S. aureus* cell suspensions and scored after 24 h incubation with *P. aeruginosa* culture supernatants. Values are the average and standard deviations of three independent experiments (two sided student t-test; * $p < 0.05$, ** $p < 0.01$, **** $p < 0.001$).

B. Secondary metabolites from the indicated strains were quantified by metabolomic analysis and represented in the heat map compared to the values of the $\Delta wspF$ mutant set to 100% (white).

C. Biofilm formation was determined after 12 h incubation in M14 medium at 37°C by crystal violet staining. The c-di-GMP degrading phosphodiesterase gene PA14_36990 was constitutively expressed from plasmid pPDE.

D. *S. aureus* killing activity of culture supernatants was determined by plate counts after 24 h incubation. Values are the average and standard deviations of three independent experiments (two sided student t-test, **** $p < 0.001$). [Color figure can be viewed at wileyonlinelibrary.com]

(Castric and Castric, 1983) was detectable in the $\Delta wspF$ mutant, but not in the PA14 wild type and the $\Delta wsp\Delta hcn$ mutant (Fig. S3A). The Δhcn mutant generated in the $\Delta wspF$ background showed a 10-fold increase in *S. aureus* viable counts, suggesting a moderate contribution of HCN in *S. aureus* killing (Fig. S3B).

To assess the impact of the generated deletions in the $\Delta wspF$ mutant on the metabolome, we submitted their supernatants to metabolomics analysis. As expected, pyochelin and/or pyoverdine were undetectable in the $\Delta wspF\Delta pchAD$ and $\Delta wspF\Delta pchAD\Delta pvdL$ mutants. Similarly, rhamnolipids and the four AQNOs were absent in supernatants of the $\Delta wspF\Delta rhIA$ and $\Delta wspF\Delta pqsL$ mutants respectively (Fig. 2B). Pyocyanin levels were unaffected in the biosynthesis mutants and were comparable to those of the wild type and the $\Delta wspF$ mutant (Fig. S2E). Surprisingly, we observed two to threefold decreased amounts of the four AQNOs and the quorum-sensing (QS) signalling molecules 3-oxo-C12-HSL and PQS in the $\Delta wspF\Delta rhIA$ mutant compared to the parental $\Delta wspF$ mutant. A possible explanation is that rhamnolipids promote the incorporation of these hydrophobic molecules into outer membrane vesicles (Mashburn-Warren *et al.*, 2008). Hence, in the absence of rhamnolipids, AQNOs and 3-oxo-C12-HSL may remain attached to the bacterial membrane thereby decreasing their concentrations in the supernatants. Altogether, our combined genetic and biochemical analyses demonstrate that the four compound clusters identified by metabolomics to be overexpressed in the $\Delta wspF$ mutant, all contribute to *S. aureus* killing.

Expression of secreted killing factors is QS-dependent and not regulated by c-di-GMP

A hallmark of the $\Delta wspF$ mutant is the constitutive activation of the WspR cyclase through phosphorelay systems, increasing c-di-GMP levels responsible for increased biofilm formation and the characteristic wrinkly colony morphology (Hickman *et al.*, 2005). We wondered whether increased levels of c-di-GMP would also trigger *S. aureus* killing activity in the $\Delta wspF$ mutant. We thus cloned the gene of the phosphodiesterase (PDE) PA14_36990, which hydrolyzes c-di-GMP (Kulasakara *et al.*, 2006; Hickman and Harwood, 2008) and introduced the resulting plasmid pPDE in PA14 and in the $\Delta wspF$ mutant. As expected pPDE expression decreased biofilm formation of the $\Delta wspF$ mutant by 50% (Fig. 2C). In contrast, pPDE expression did not affect the *S. aureus* killing activity of a $\Delta wspF$ mutant (Fig. 2D), nor did it affect siderophore production (data not shown). Hence, c-di-GMP levels do not seem to play a role in the killing activity of the $\Delta wspF$ mutant.

Because rhamnolipid and AQNO synthesis is QS-controlled, we hypothesized an upregulation or advanced expression of the *P. aeruginosa* QS system(s) in the

$\Delta wspF$ mutant. To determine the onset of the killing activity in the supernatants, we collected supernatant samples during static growth in microtitre plates. The *S. aureus* killing activity occurred after 6 h growth (mid-log phase) in the $\Delta wspF$ mutant supernatants, and increased until stationary phase was reached (data not shown). No killing activity was observed in the PA14 supernatants under these conditions, although PA14 reached similar cell densities. Surprisingly, we observed decreased amounts of the *las*-system QS molecule 3-oxo-C12-HSL (Fig. 2B and S2F) and of the PQS signalling molecule (Figs 2B and S2H) in the $\Delta wspF$ mutant compared to the wild type. In contrast, the metabolomics analysis showed a two-fold increase in signal intensity for the *rhl*-QS-system signalling molecule C4-HSL in the $\Delta wspF$ mutant supernatant compared to PA14 (Fig. 2B), which was corroborated by a three-fold higher expression of the *rhlI* gene, encoding the C4-HSL synthase (Fig. S2G). We therefore suspect that increased or advanced expression of the C4-HSL dependent *rhl*-QS system might explain the increase in rhamnolipid production in the $\Delta wspF$ supernatant.

Secreted factors display distinct killing phases

To determine whether the compounds overproduced by the $\Delta wspF$ mutant act simultaneously or sequentially, we exposed *S. aureus* cells to culture supernatants of *P. aeruginosa* mutants constructed in the $\Delta wspF$ background and followed *S. aureus* survival during 24 h (Fig. 3A). As our previous data showed overproduction of several secreted proteins in the $\Delta wspF$ supernatant (Tognon *et al.*, 2017), including the staphylococcal protease LasA (Kessler *et al.*, 1997), we also tested a $\Delta wspF\Delta lasA$ mutant. This allowed us to distinguish three killing phases. During the initial phase (0–2 h), *S. aureus* viable counts declined rapidly in all supernatants with the exception of the one from the $\Delta wspF\Delta lasA$ mutant (Fig. 3A, green rectangle and zoomed blue box). During the second phase (2–6 h), *S. aureus* CFUs decreased for all supernatants by 1 to 2-logs (Fig. 3A, blue rectangle). During the third phase (6–24 h), a further 1 to 2-log decrease in CFUs occurred except for supernatants from PA14 and the $\Delta wspF\Delta pqsL$ and $\Delta wspF\Delta pchAD\Delta pvdL$ mutants (Fig. 3A, yellow rectangle). We conclude that the first killing phase (0–2 h) is mainly dependent on the LasA protease. The second phase (2–6 h) is initially dominated (2–4 h) by the action of rhamnolipids (CFU remain stable in the $\Delta wspF\Delta rhIA$ mutant), whereas the third phase (6–24 h) involves AQNOs, as well as both pyochelin and pyoverdine. This complex scheme suggests an initial lysis of a subpopulation of *S. aureus* cells, followed by a combined and probably synergistic action among rhamnolipids, AQNOs and siderophores.

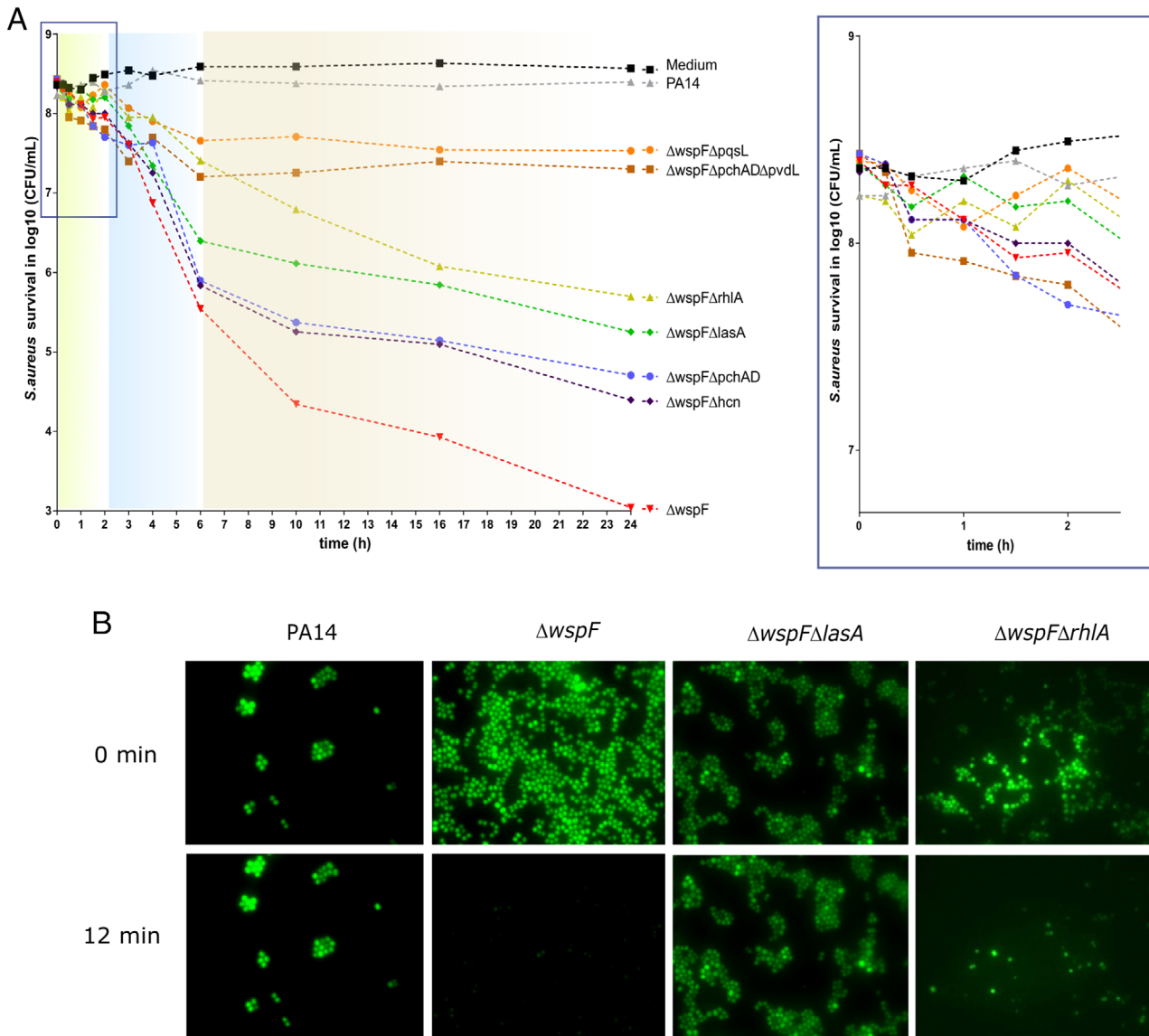


Fig 3. Survival kinetics and microscopic analysis reveal three killing phases in $\Delta wspF$ supernatants.

A. Killing activity of crude supernatants from PA14, $\Delta wspF$ mutant and derivatives was monitored during 24 h (left panel), a blow up is shown for the initial 2.5 h (right panel). The fast killing phase (light green background), resulting mainly from the LasA protease is followed by a second rhamnolipid dependent phase (blue background) and a third phase mainly dependent on HCN, pyochelin and HQNO (beige background).

B. GFP-labelled *S. aureus* Newman cells were incubated for 12 min with filtered culture supernatants from the indicated strains and analysed under a fluorescent microscope for cell lysis. [Color figure can be viewed at wileyonlinelibrary.com]

To verify that the initial drop in CFU resulted indeed from cell lysis, we examined GFP-labelled *S. aureus* cells under the microscope. Indeed the $\Delta wspF$ mutant supernatant lysed *S. aureus* cells within 12 min, although no lysis was observed with PA14 and $\Delta wspF\Delta lasA$ mutant supernatants, confirming that initial lysis was due to the action of the LasA protease (Fig. 3B). Rhamnolipids were not involved in cell lysis because supernatants from the $\Delta wspF\Delta rhIA$ mutant still showed *S. aureus* lysis (Fig. 3B) and addition of commercial rhamnolipids to M14 medium at concentrations of up to 400 $\mu\text{g ml}^{-1}$ did not cause

S. aureus cell lysis (data not shown). These data support a cell-permeabilizing role of rhamnolipids during later stages of the killing process.

We further investigated the antibacterial properties of the supernatants by measuring ROS generation. *S. aureus* cells exposed to the PA14 or $\Delta wspF$ supernatants showed identical hydroxyl radical production during the first 4 h. However, in the presence of PA14 supernatant, hydroxyl radicals reached a plateau level after 9 h, whereas in the presence of $\Delta wspF$ supernatant the hydroxyl radical production showed a steady increase,

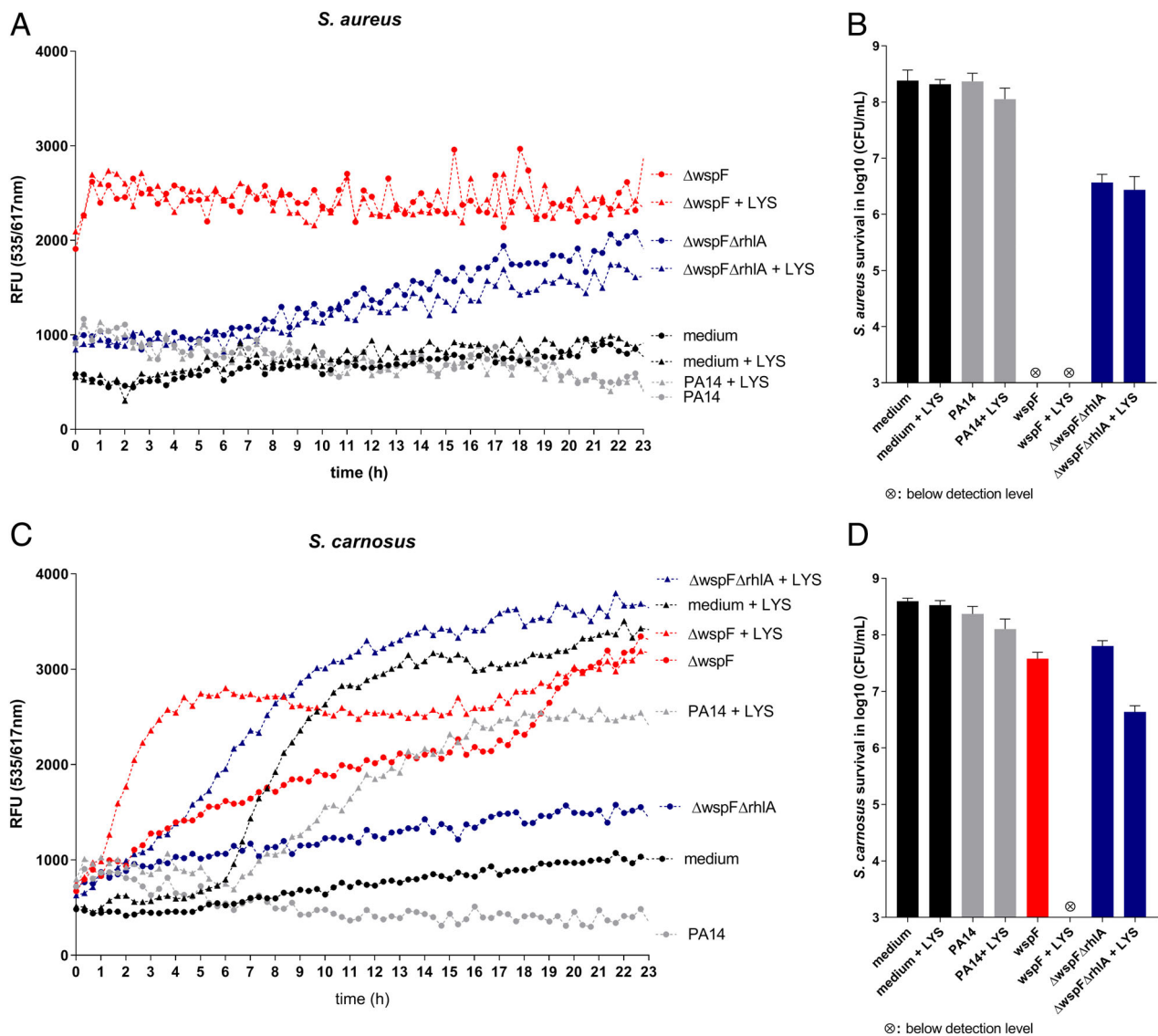


Fig 4. Effect of rhamnolipids and lysozyme on staphylococcal membranes.

A. Propidium iodide (PI) fluorescence was measured in *S. aureus* Newman in the presence or absence of rhamnolipids ($250 \mu\text{g ml}^{-1}$) and lysozyme ($100 \mu\text{g ml}^{-1}$) in static incubation at 37°C . PI fluorescence was monitored in a Biotek Synergy H1 plate reader (ex 535 nm/em 617 nm).

B. Survival of *S. aureus* was determined by serial dilution and CFU counts on LB agar plates after the 23 h incubation period.

C. PI fluorescence was measured in *S. carnosus* in the presence or absence of rhamnolipids ($250 \mu\text{g ml}^{-1}$) and lysozyme ($100 \mu\text{g ml}^{-1}$) as described above.

D. Survival of *S. carnosus* was determined by serial dilution and CFU counts on LB agar plates at the end of the incubation period. Data represent background-deducted values (supernatants with PI but no bacterial cells) and are the mean of technical triplicates. [Color figure can be viewed at wileyonlinelibrary.com]

reaching a four-fold higher level compared to PA14 supernatants after 24 h (Fig. S4). The Δ wspF Δ pvdL and Δ wspF Δ pchAD Δ pvdL mutant supernatants deficient for pyoverdine and/or pyochelin production respectively showed a slower onset and reduced ROS production compared to those of the Δ wspF mutant at 24 h, suggesting the role of iron availability in the generation of hydroxyl radicals via the Fenton reaction. The signal for superoxide production was weak and did not show any significant differences between the supernatants (data not shown). The data suggest that the two siderophores

pyoverdine and pyochelin, overproduced in the Δ wspF mutant, play a role in hydroxyl radical production and likely contribute to the later killing phases (Fig. 3A).

Rhamnolipids increase staphylococcal cell permeability

To assess the effect of rhamnolipids on *S. aureus* cell permeability, we used propidium iodide (PI) fluorescence. PI emits fluorescence when intercalating into DNA but cannot penetrate intact cell membranes. *S. aureus* strain Newman, exposed to medium or PA14 supernatant,

showed no change in PI-fluorescence during the incubation period (Fig. 4A, grey and black symbols). However, in the presence of the $\Delta wspF$ supernatant, PI-fluorescence increased rapidly during the first 60 min and reached a fourfold higher level than in the medium control (Fig. 4A, red dots), indicating fast cell permeabilization. At the end of the incubation, viable cell counts dropped by 5-logs under these conditions (Fig. 4B). Incubation with the rhamnolipid-deficient $\Delta wspF\Delta rhIA$ supernatant showed a linear increase in PI-fluorescence reaching twice the level of the medium control (Fig. 4A, blue dots). The $\Delta wspF\Delta rhIA$ supernatant showed only a 2-log decrease in viable *S. aureus* cell counts (Fig. 4B). *S. aureus* possesses a lysozyme-resistant cell wall due to O-acetylation of its peptidoglycan; hence, addition of lysozyme to the supernatants had no additional effect on PI-fluorescence or cell viability.

To assess whether the permeabilizing activity was specific to *S. aureus*, we repeated the experiment with *S. carnosus*, which has a lysozyme susceptible peptidoglycan. Although medium or PA14 supernatant alone showed no increase in PI-fluorescence (Fig. 4C, grey and black dots), addition of a sub-lethal amount of lysozyme ($100 \mu\text{g ml}^{-1}$) increased PI-fluorescence after 6–7 h of incubation (Fig. 4C, grey and black triangles), reaching a plateau level after 15 h. In the presence of the $\Delta wspF$ supernatant, PI-fluorescence increased steadily (Fig. 4C,

red dots) but viable counts decreased only 10-fold compared to the medium or PA14 treatments (Fig. 4D). Interestingly, PI-fluorescence showed a rapid exponential increase when we added lysozyme to the $\Delta wspF$ supernatant (Fig. 4C, red triangles), which resulted in a drastic 5-log reduction of *S. carnosus* CFUs (Fig. 4D). As observed for *S. aureus*, no PI-fluorescence increase occurred with the $\Delta wspF\Delta rhIA$ mutant supernatant (Fig. 4C, blue dots), supporting the permeabilizing action of rhamnolipids also in *S. carnosus*. Finally, addition of lysozyme to the $\Delta wspF\Delta rhIA$ mutant increased PI-fluorescence (Fig. 4C, blue triangles), resulting in a concomitant 10-fold decrease in *S. carnosus* CFUs (Fig. 4D). Hence, rapid permeabilization by rhamnolipids, in the absence (*S. aureus*) or the presence (*S. carnosus*) of lysozyme, is crucial to cause irreversible cell damage and killing by the factors present in the $\Delta wspF$ supernatants.

Formulation of a lethal synthetic cocktail from *P. aeruginosa* metabolites

We next tested whether the compounds identified by the metabolomic analysis would be sufficient to cause bacterial killing, when reconstituted in M14 medium at concentrations close to those identified in the $\Delta wspF$ supernatant ($250 \mu\text{g ml}^{-1}$ rhamnolipids, $4 \mu\text{M}$ HQNO, $10 \mu\text{M}$ pyochelin and $6 \mu\text{M}$ pyoverdine). Added individually to the medium at

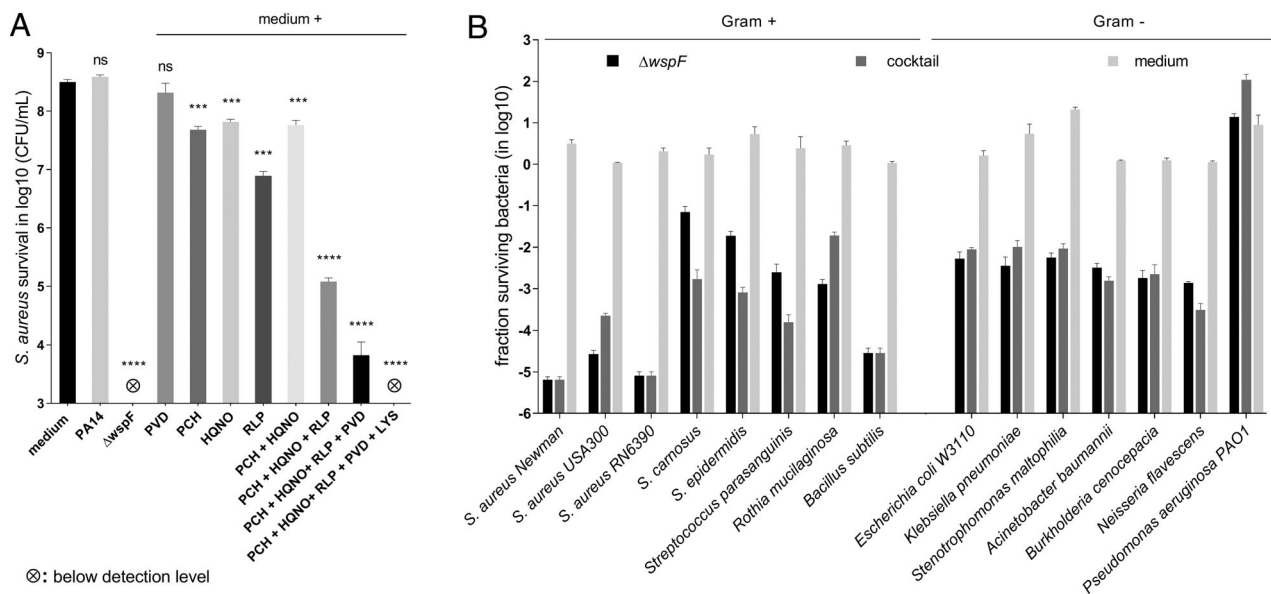


Fig 5. Formulation of the antibacterial cocktail and its broad-spectrum activity.

A. Compounds identified by metabolomics in the $\Delta wspF$ supernatant were added individually and in combination to M14 medium at the following final concentrations: HQNO ($4 \mu\text{M}$), pyochelin (PCH, $10 \mu\text{M}$), rhamnolipids (RLP, $250 \mu\text{g ml}^{-1}$), pyoverdine (PVD, $6 \mu\text{M}$) and lysozyme (LYS, $100 \mu\text{g ml}^{-1}$). Viable counts of *S. aureus* Newman strain were determined after 24 h incubation. Statistical analysis was performed using Student's *t* test. All conditions were compared to medium control.

B. Bacterial strains were grown to exponential phase and adjusted to 10^8 CFU ml^{-1} in M14 medium. Bacterial suspensions were incubated for 24 h with $\Delta wspF$ supernatant, synthetic cocktail (RLP, pyochelin, HQNO, siderophore, lysozyme) or M14 medium. Cell survival was determined by CFU counts. Results are the average and standard deviation of technical duplicates of one experiment repeated twice with similar results. [Color figure can be viewed at wileyonlinelibrary.com]

these concentrations only rhamnolipids showed at most a 50-fold reduction in *S. aureus* survival (Figs 5A and S5A). HQNO and pyochelin added either alone or in combination did not affect significantly *S. aureus* survival (Figs 5A and S5B and C). However, addition of rhamnolipids to HQNO and pyochelin increased *S. aureus* killing by 3-logs, suggesting a synergistic action of these three compounds. Pyoverdine further decreased *S. aureus* CFUs by 1-log. Lysozyme alone at 100 $\mu\text{g ml}^{-1}$ had no effect on *S. aureus* killing (Fig. 4B), whereas it further reduced CFU counts below our detection limit in the presence of the cocktail (Fig. 5A). Hence, the four metabolites identified by metabolomics all contribute to *S. aureus* killing and the cocktail showed a similar bactericidal activity as the one of the $\Delta wspF$ supernatant (Fig. 5A). To assess the specificity of the iron chelators, we substituted pyoverdine by the siderophore enterobactin from *E. coli* and protochelin from *Azotobacter vinelandii* or by the synthetic iron chelator 2,2'-dipyridyl. All of them enhanced the killing activity to a similar level as pyoverdine (Fig. S5D), suggesting that the Fe(III) chelating function was essential for the killing activity.

We used this cocktail, containing 2,2'-dipyridyl and lysozyme, to test its activity on other Gram-positive and Gram-negative bacteria. We found that the cocktail showed similar or even better activity than the $\Delta wspF$ supernatant against six Gram-positive and six Gram-negative bacterial species, including several respiratory isolates (*Rothia mucilaginosa*, *Neisseria flavescens*, *Streptococcus parasanguinis*) (Fig. 5B) as well as Gram-negative non-fermenters. All bacterial species showed at least a 2 to 3-log reduction in viable counts, suggesting that the targets of the cocktail components are conserved among distantly related bacterial species. As expected, the cocktail did not affect viability of *P. aeruginosa* (Fig. 5B).

Discussion

Our unbiased metabolomic comparison between a $\Delta wspF$ and PA14 wild type supernatant allowed us to identify specific *P. aeruginosa* metabolites, which individually showed no antibiotic activity, but when combined in a synthetic cocktail, resulted in a broad-spectrum bactericidal activity. An essential component of this cocktail were rhamnolipids, produced by *Pseudomonas* and *Burkholderia* spp (Soberon-Chavez et al., 2005). Their main function seems to be the solubilization of hydrophobic compounds such as aliphatic C-sources acquired from the environment (Noordman and Janssen, 2002) or the self-produced PQS-signalling molecule (Calfee et al., 2005). Rhamnolipids show intrinsic antimicrobial activity against both Gram-positive and Gram-negative bacteria (Haba et al., 2003; Nitschke et al., 2010; Samadi et al., 2012), as well as amoeba (Cosson et al., 2002)

and fungi (Goswami et al., 2015). These glycolipids also display surfactant activity (Abdel-Mawgoud et al., 2009), required for swarming motility (Köhler et al., 2000), disrupt tight junctions in epithelial cells (Zulianello et al., 2006) and lyse polymorphonuclear neutrophils (Jensen et al., 2007). The amounts produced by the $\Delta wspF$ mutant ranged between 300 and 400 $\mu\text{g ml}^{-1}$, a concentration reported to have bacteriostatic activity against *S. aureus*, *S. epidermidis* and *B. subtilis* (Haba et al., 2003; Nitschke et al., 2010; Samadi et al., 2012). However, incubation with a commercial mix of rhamnolipids at concentrations of up to 500 $\mu\text{g ml}^{-1}$ caused only a modest 50-fold reduction in *S. aureus* and *S. carnosus* viable counts, which did not result from cell lysis as we confirmed by microscopic analysis. These data support the notion that at the concentrations detected in the $\Delta wspF$ supernatant, rhamnolipids alone are not sufficient to explain a 5 to 6-log decrease in *S. aureus* viable cell counts. We therefore conclude that rhamnolipids act mainly as a permeabilizing agent (Radlinski et al., 2017). Rhamnolipids can form micelles, which might incorporate cargo molecules, like the hydrophobic AQNOs and pyochelin (Fig. 6). Along this line, the QS signals PQS and 3-oxo-C12-HSL were shown to be integrated into outer membrane vesicles of *P. aeruginosa*, thereby promoting their dissemination within a bacterial community (Mashburn-Warren et al., 2008). Membrane vesicles of *P. aeruginosa* were reported to fuse to the membranes of other Gram-negative bacteria and even to *S. aureus* membranes (Kadurugamuwa and Beveridge, 1996). Whether this is the case for rhamnolipid micelles remains to be determined. The critical micellar concentration for rhamnolipids is approximately 100 $\mu\text{g ml}^{-1}$ (Klosowska-Chomiczewska et al., 2017), a concentration below the 300–400 $\mu\text{g ml}^{-1}$ measured in $\Delta wspF$ supernatants. Hence, the majority of rhamnolipid molecules in the $\Delta wspF$ supernatant should be under the form of micelles. Indeed, preliminary experiments using Nile Red to stain rhamnolipid micelles are in agreement with this hypothesis (our own unpublished observations). In the case of *S. carnosus*, lysozyme could further enhance the access of outer membrane vesicles or rhamnolipid micelles to the cytoplasmic membrane.

AQNOs represent another family of specialized metabolites reported to have anti-staphylococcal activity. In particular, HQNO and NQNO (Lightbown and Jackson, 1954; Machan et al., 1992; Szamosvari and Bottcher, 2017) inhibit cytochrome oxidases of the electron transport chain (CydAB in *S. aureus*) by blocking the access to respiratory quinones (menadione) (Voggu et al., 2006). HQNO also selects small colony variants in *S. aureus*, which carry mutations in heme or menadione synthesis pathways (Hoffman et al., 2006). AQNOs are produced *in vitro* by CF-isolates in the range of 1–10 μM (Nguyen et al., 2016),

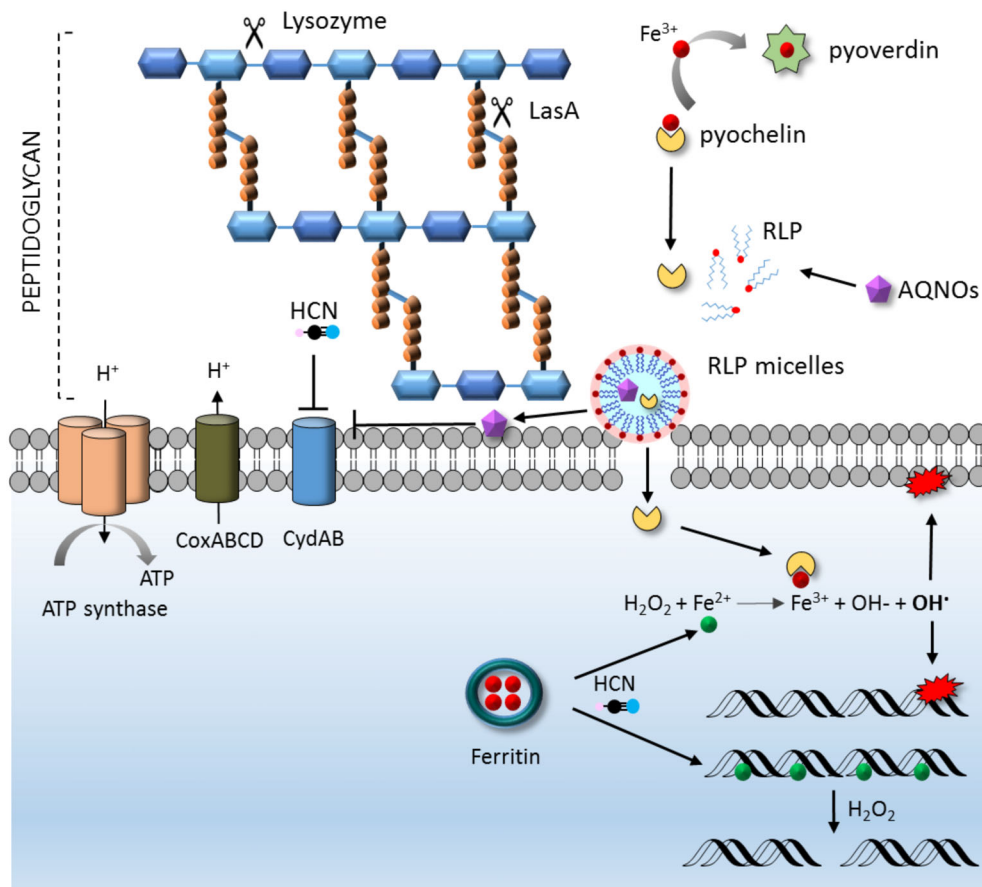


Fig 6. Proposed scheme for the action of compounds identified in the $\Delta wspF$ mutant supernatant.

HQNO and likely other AQNOs inhibit binding of menadione to CydAB cytochrome oxidase. HCN blocks heme binding in CydAB and favors release of Fe from Fe-S clusters and ferritins. Siderophores with higher Fe(III)-affinity than pyochelin could capture Fe(III) outside the cell to generate apo-pyochelin. Rhamnolipids (RLP) form micelles and deliver apo-pyochelin and AQNOs to the cell membrane. Pyochelin increases intracellular ROS production by chelating Fe(III) generated during the Fenton reaction. This leads to DNA and membrane damage or DNA fragmentation in the presence of H_2O_2 [Color figure can be viewed at wileyonlinelibrary.com]

but were also detected in lung biopsies from CF-patients (Garg *et al.*, 2017). Indeed, the $\Delta wspF\Delta pqsL$ mutant deficient in AQNO production, as shown by the metabolome analysis, showed strongly diminished killing activity. PqsL is responsible for the hydroxylation of the AQs to generate AQNOs (Drees *et al.*, 2018). Addition of commercial HQNO alone had only a weak antimicrobial effect on *S. aureus*, suggesting that HQNO requires other components present in the $\Delta wspF$ supernatant. We cannot exclude that AQNOs with longer acyl chains (NQNO, DQNO, UQNO) or harbouring an unsaturated acyl chain (Szamosvari and Bottcher, 2017) detected in our extended metabolomics analysis, also participate in the killing activity. Interestingly, the activity of HQNO seems to increase under iron-deficient conditions (Nguyen *et al.*, 2016), which pinpoints the potential role of siderophores in our cocktail. Surprisingly, we could demonstrate killing of *S. carnosus*, which in contrast to *S. aureus* expresses a cyanide and HQNO insensitive CydB enzyme and has a lysozyme-

susceptible peptidoglycan (Bera *et al.*, 2006; Voggu *et al.*, 2006). This would incriminate other compounds present in the $\Delta wspF$ supernatant and acting on a different *S. carnosus* target. Alternatively, CydB might be susceptible to long-chain AQNOs, which do not gain access to its target in the absence of lysozyme treatment.

Besides the QS-controlled factors rhamnolipids and AQNOs, the $\Delta wspF$ mutant also overproduced the main siderophores pyochelin and pyoverdinin. Pyochelin has been reported to have bacteriostatic effects on *S. aureus* and other bacterial species and was suggested to generate reactive oxygen species (Adler *et al.*, 2012; Ong *et al.*, 2017) in the presence of pyocyanin (Coffman *et al.*, 1990; Britigan *et al.*, 1992). We could show here that pyochelin participates in *S. aureus* killing because the pyochelin-deficient *pchAD* mutant showed decreased killing activity and addition of pyochelin at 200 μM resulted in a 2-log reduction in *S. aureus* viable counts, both in medium and in PA14 supernatant. In *E. coli*,

addition of catechol siderophores (enterobactin) was shown to abrogate ROS induced damage generated by pyochelin (Adler *et al.*, 2012). However, in our study, we observed the opposite effect since (i) addition of pyoverdine (a cyclic peptide harbouring a dihydroxy quinoline chelating group) to the pyochelin containing cocktail increased *S. aureus* killing activity by 3-logs and (ii) deletion of pyoverdine synthesis genes in the pyochelin deficient $\Delta wspF\Delta pchAD$ strain decreased killing activity of the corresponding supernatants by 3-logs. We hypothesize that pyoverdine, which has a higher affinity for iron than pyochelin, chelates Fe(III) outside the cell generating apo-pyochelin (Fig. 6). In Gram-negative bacteria, TonB-dependent receptor proteins actively transport siderophores across the outer membrane, whereas Gram-positive bacteria lack these transporters. We therefore suggest that the hydrophobic apo-pyochelin is captured by membrane vesicles or rhamnolipid micelles, which eventually fuse with the membrane of target bacteria and deliver pyochelin into the cytosol. The other high-affinity iron chelators tested (enterobactin, protochelin, 2,2'-dipyridyl) also increased the killing activity supporting the role of iron chelation for bactericidal activity. The high-affinity siderophores could remove Fe(III) generated during the Fenton reaction thereby increasing the production of hydroxyl radicals (Fig. 6).

In summary, our data show that *P. aeruginosa* produces a set of metabolites, including respiratory chain inhibitors (AQNOs, HCN), siderophores (pyochelin, pyoverdine) involved in ROS production, and cell permeabilizers (rhamnolipids, LasA protease), which when combined synthetically, result in an efficient broad-spectrum bactericidal cocktail. Hence, *P. aeruginosa* uses a probably unique combination of effector and membrane permeabilizing compounds, targeting a broad spectrum of Gram-positive and Gram-negative bacteria. Secretion of this lethal cocktail is likely beneficial to *P. aeruginosa* when establishing or defending niches in the environment or in the host.

Experimental procedures

Bacterial strains, growth conditions and supernatant preparation

Bacterial strains, plasmids and primers used in this study are listed in Table S1. M14 medium was adapted from the literature (Rudin *et al.*, 1974) and is based on M9 salts (Na_2HPO_4 6 g L⁻¹; KH_2PO_4 3 g L⁻¹; NaCl 0.5 g L⁻¹; NH_4Cl 1 g L⁻¹) supplemented with casamino acids (BD™) 10 g L⁻¹, magnesium sulfate ($\text{MgSO}_4 \cdot 7\text{H}_2\text{O}$) 1 mM, thiamine (vitamin B1) 2 mg L⁻¹, niacin (vitamin B3) 2 mg L⁻¹, calcium pantothenate (vitamin B5) 2 mg L⁻¹, biotin (vitamin B9) 0.1 mg L⁻¹ and glucose 2 g L⁻¹. Casamino acids, vitamins and glucose solutions were sterilized by

filtration and stored separately at 4°C. M9 salts and magnesium sulfate were sterilized by autoclaving at 121°C for 15 min (Tognon *et al.*, 2017). Supernatants of bacterial cultures were recovered after 24 h of static growth at 37°C in microtitre plates (TPP, Switzerland). The cultures were pooled and centrifuged at 8000 rpm for 5 min. Supernatants were sterilized by filtration (0.22 µm filters, Millipore, Switzerland) and stored at -20°C.

Mass spectrometry analysis

Metabolite profiling was performed on an Acquity UPLC system (Waters, Milford, MA) interfaced to a high-resolution Q-Exactive Focus mass spectrometer (Thermo Scientific, Bremen, Germany), using a heated electrospray ionization (HESI-II) source. The LC conditions were as follows: column: Waters BEH C18 100 × 2.1 mm, 1.7 µm; mobile phase: (A) water with 0.1% formic acid; (B) acetonitrile with 0.1% formic acid; flow rate: 500 µl min⁻¹; injection volume: 1 µl; gradient: isocratic at 2% B for 0.2 min followed by a linear gradient of 2–100% B over 11 min and isocratic at 100% B for 3 min, return to initial condition in 0.2 min and equilibration step for 2.4 min. In positive ion mode, diisooctyl phthalate $\text{C}_{24}\text{H}_{38}\text{O}_4$ ($\text{M} + \text{H}$)⁺ ion (m/z 391.28429) was used as internal lock mass. The optimized HESI-II parameters were the following: source voltage: 3.5 kV (pos), sheath gas flow rate (N2): 48 units; auxiliary gas flow rate: 11 units; spare gas flow rate: 2.0; capillary temperature: 256.2°C (pos), S-Lens RF Level: 45. The mass analyser was calibrated using a mixture of caffeine, methionine-arginine-phenylalanine-alanine-acetate (MRFA), sodium dodecyl sulfate, sodium taurocholate and Ultramark 1621 in an acetonitrile/methanol/water solution containing 1% formic acid by direct injection. The data-dependent MS/MS events were performed on the three most intense ions detected in full scan MS (Top3 experiment). The MS/MS isolation window width was 1 Da, and the normalized collision energy (NCE) was set to 15, 30 and 45 units. In data-dependent MS/MS experiments, full scans were acquired at a resolution of 35,000 FWHM (at m/z 200) and MS/MS scans at 17500 FWHM both with an automatic maximum injection time. After being acquired in the MS/MS scans, parent ions were placed in a dynamic exclusion list for 2.0 s.

Metabolomics and mass spectrometry data treatment

PA14 and $\Delta wspF$ mutant supernatants were profiled by UHPLC coupled to a Q-Exactive Focus Mass-spectrometer with automated acquisition of MS/MS spectra. The MS data were converted from .RAW (Thermo) standard data format to .mzXML format using the MSConvert software, part of the ProteoWizard package (Chambers *et al.*, 2012). The converted files were treated using the MZMine software suite v. 2.39 (Pluskal *et al.*, 2010). The dereplication

strategy consisted of a combination of molecular networking and an *in silico* generated fragmentation database spectral matching, informed by taxonomic information (Rutz *et al.*, 2019). Dereplication results were then visualized as chemical structures, and their relative abundance in both samples was estimated as previously described (Allard *et al.*, 2016). Unsupervised and supervised statistical analyses (PCA and OPLS_DA) of the metabolomics data was used to highlight differentially expressed compounds using the R *ropis* package (<https://doi.org/10.18129/B9.bioc.ropis>). Only compounds present in the $\Delta wspF$ mutant at increased levels compared to the wild type were specifically investigated.

Molecular networks generation

The molecular network was created using the online workflow at GNPS (<http://gnps.ucsd.edu>). A network was then created where edges were filtered to have a cosine score above 0.7 and more than six matched peaks. Further edges between two nodes were kept in the network if and only if each of the nodes appeared in each other's respective top 10 most similar nodes. The spectra in the network were then searched against GNPS spectral libraries. All matches kept between network spectra and library spectra were required to have a score above 0.6 and at least six matched peaks. To separate isomers and consider semi-quantitative information, a Feature-Based Molecular Networking workflow was followed (Nothias *et al.*, 2019). The molecular networking parameters and the complete results are accessible on the GNPS platform at the following address: <https://gnps.ucsd.edu/ProteoSAFe/status.jsp?task=a85e2cb7e0c84ab3a739e0b46e86ef73>. The molecular network and the associated ISDB-DNP annotations are provided as a .cys file in Supplementary Material. This network file can be opened using Cytoscape (<https://cytoscape.org/download.html>).

Quantification of specialized metabolites

Rhamnolipid quantification was performed as described (Wittgens *et al.*, 2011) with slight modifications. Samples containing 2 ml of filtered supernatant were treated with equal volumes of ethyl acetate. A standard curve was established by dissolving a mix of mono and di-rhamnolipids (R90-10G, Sigma Aldrich, Switzerland) in 2 ml ddH₂O and subsequent extraction with equal volumes of ethyl acetate. After vortexing for 1 min, samples were centrifuged for 1 min at 5000 rpm to separate the phases. The organic solvent was evaporated in a SpeedVac (Thermo Scientific), and residues containing rhamnolipids were resuspended in 100 μ l of ddH₂O and mixed with an equal volume of 1.6% orcinol (Sigma Aldrich, Switzerland) in ddH₂O. Of note, 800 μ l of 60% sulphuric acid (vol/vol) was added, and samples were

incubated for 45 min at 80°C. Then, 100 μ l of the reaction mix were transferred to a microtitre plate, and OD₄₂₀ was measured in a Synergy H1 Multi-Mode plate reader (BioTek®). For graphic representation, the background level of medium absorbance was subtracted.

Measurement of pyoverdinin in supernatants was performed as described (Hoegy *et al.*, 2014). Of note, 100 μ l of filtered supernatants were transferred to a microtitre plate, and fluorescence was measured in a Synergy H1 Multi-Mode plate reader (BioTek®) with excitation at 400 nm and emission at 460 nm. For graphic representations, fluorescence values were divided by OD₆₀₀ of culture from which supernatants were obtained.

Measurement of relative levels of pyochelin produced by *P. aeruginosa* was performed as described with some modifications (Hoegy *et al.*, 2014). Five millilitres of sterile supernatant was adjusted to pH = 3.0 by adding solid citric acid. Ten millilitres CH₂Cl₂ was added to the acidified supernatant, and pyochelin was extracted by vortexing the 50 ml falcon tube for 1 min. The organic phase was collected and dried under a nitrogen flow overnight. The residue was resuspended in 1 ml 100 mM Tris-HCl buffer (pH 8) and used for pyochelin detection by spectrofluorometry or stored at -20°C. Of note, 200 μ l of the suspension was transferred to a microtitre plate, and pyochelin fluorescence (ex 355 nm/em 430 nm) was determined in duplicates. Relative levels of pyochelin were expressed as RFU/OD₆₀₀. HCN production by growing *P. aeruginosa* cultures was performed as described (Castric and Castric, 1983), except that the filter paper was placed above a microtitre plate well during growth in M14 medium.

Pyocyanin in *P. aeruginosa* supernatants was quantified as previously described (Frank and Demoss, 1959; Köhler *et al.*, 2014). Of note, 0.5 ml of CHCl₃ was added to 0.75 ml of supernatant and vortexed for 30 s. After centrifugation (2 min at 13,000 rpm), the lower organic phase containing pyocyanin was transferred to a new tube. Then, 0.5 ml of 0.2 N HCl was added and tube was vortexed for 30 s. Two hundred microlitres were transferred to a microtitre plate. Relative levels of pyocyanin were expressed as ratio OD₅₂₀/OD₆₀₀.

Measurement of 3-oxo-C12-HSL was performed using *E. coli* JM109 strain, harbouring the bioluminescence reporter plasmid pSB1075 (*placI::luxCDABE*, *lasR*). Briefly, JM109 (pSB1075) (Winson *et al.*, 1998) was grown overnight in LB medium supplemented with 50 μ g ml⁻¹ ampicillin. Overnight culture was diluted 1:10 in LB medium. Of note, 190 μ l of diluted cell suspension was distributed in a microtitre plate, and 10 μ l of supernatant was added. Bioluminescence was measured using the kinetic program in a BioTek Synergy H1 plate reader.

Measurement of PQS was performed using the PAO1 biosensor strain ($\Delta pqsA$ mutant harbouring a chromosomal CTX-*pqsA::luxCDAB* fusion) (Fletcher *et al.*, 2007).

Briefly, the PQS biosensor strain was grown overnight in LB medium. Next day the biosensor strain culture was adjusted to $OD_{600} = 1.0$ and diluted 1:50. Then, 100 μl of the test bacterial supernatant was distributed into a 96 well plate and mixed with 100 μl of the diluted biosensor strain. Bioluminescence was measured using the kinetic program in a BioTek plate reader and expressed as relative light units (RLU) per OD_{600} .

Killing assays

Killing assays were performed on *S. aureus* cells grown for 6 h in M14 medium under static growth conditions in microtitre plates (Tognon *et al.*, 2017). After the 6 h incubation, 100 μl of *S. aureus* culture was removed and replaced with either 100 μl M14 medium or *P. aeruginosa* supernatant. Growth (OD_{600}) was monitored in a plate reader (BioTek®) for 24 h. Viable plate counts were performed to determine survival *S. aureus* cells. Other bacterial strains were grown on LB-plates or specific growth media. Cells were scraped from the plate, and a suspension was prepared and adjusted to obtain 10^8 CFU ml^{-1} . After 24 h incubation in the presence of culture supernatants, surviving cells were determined by plate counts.

Reactive oxygen species detection

Reactive oxygen species (ROS) were measured using the total ROS/Superoxide Detection Kit (Enzo Life Science, Farmingdale, NY) according to the manufacturer's instructions with slight modifications. Briefly, ROS and oxidative stress of cell suspensions were detected by staining with the two fluorescent dyes from the ROS detection kit. *S. aureus* cells were grown for 6 h in M14 medium under static growth conditions in microtitre plates as described (Tognon *et al.*, 2017). At that point, 100 μl of *S. aureus* culture was removed and replaced with either 100 μl M14 medium, *P. aeruginosa* supernatant. A 50 μl aliquot of M14 medium containing the two fluorescent dyes was added to each well (8.75 μM final conc.). Fluorescence of the fluorescein (ROS) (ex 488 nm/em 520 nm) and rhodamine-based (superoxide) dyes (ex 550 nm/em 610 nm) was monitored in a plate reader (Synergy 1, BioTek®) every 15 min for 24 h.

Cell permeabilization measurement

S. aureus and *S. carnosus* cells were grown for 6 h in M14 medium under static growth conditions in microtitre plates. At that point, 100 μl of bacterial culture was removed and replaced with either 100 μl M14 medium or crude, filtered *P. aeruginosa* supernatants, supplemented with PI at a final concentration of 1 μM . Where indicated, lysozyme (Serva, Germany) was added at a final

concentration of 100 $\mu\text{g ml}^{-1}$. Fluorescence (ex 535 nm/em 617 nm) was monitored in a plate reader (BioTek®) every 20 min at 37°C. Kinetic curves represent background-deducted values (supernatant with PI but without bacterial cells) and are the mean of technical triplicates. At the end of the assay, viable plate counts were performed to determine bacterial survival.

Biofilm formation

Staining and quantification of biofilm was performed as described with some modifications (Coffey and Anderson, 2014). *P. aeruginosa* strains were grown in static condition in microtitre plates in M14 medium. After 20 h, planktonic cells were removed by inverting the 96-well plate. The plate was then rinsed two times with ddH_2O . Wells were stained with crystal violet (225 μl of a 0.1% solution) and incubated for 10 min. The plate was rinsed twice with ddH_2O and allowed to dry. For quantification, 150 μl 30% acetic acid was added to each well and incubated for 10 min to solubilize the biofilm. Of note, 100 μl of each sample was transferred to a new 96-well optically clear flat-bottom plate. Optical density of all samples was measured in a plate reader at 550 nm.

Construction of cyclic-guanylate-specific phosphodiesterase (PDE) expression plasmid

The coding region, including 62 bp upstream of the ATG initiation codon and 120 bp downstream of the STOP codon, was amplified with primers PA14_36990-BamHI-F and PA14_36990-HindIII-R by PCR from genomic DNA of *P. aeruginosa* PA14. The amplified 1050 bp fragment was digested with *Bam*HI-*Hind*III restriction enzymes and cloned into the expression vector pApX2 yielding plasmid pPDE. The Q5 high-fidelity DNA polymerase (NEB) was used for all amplifications. PCRs were performed in a Bio-metra PCR thermal cycler (Analytik Jena AG, Germany), using the following conditions: denaturation at 98°C for 2 min, followed by 27 cycles of 98°C for 20 s, 57°C for 30 s, 72°C for 2 min and a final extension at 72°C for 4 min. Plasmids were transferred into *P. aeruginosa* by electroporation and cells were spread on LB-agar supplemented with carbenicillin at 200 mg L^{-1} . All constructs were verified by Sanger sequencing.

Generation of P. aeruginosa knockout mutants

The generation of unmarked knockout mutants was based on the protocol described by Hoang *et al.* (Hoang *et al.*, 1998). Briefly, DNA fragments of 500–700 bps flanking the gene of interest were PCR-amplified using primer pairs F1/R1 and F2/R2 respectively (Table S1). After amplification, the obtained fragments were gel-

purified and used in a PCR fusion amplification with primers F1 and R2. For deletion of the *hcnABC* operon, a streptomycin cassette was introduced between the two flanking DNA fragments using the *Bam*HI restriction site. The resulting fusion products were gel-purified and further cloned into the suicide vector pEXG2 via *Hind*III/*Sac*I (*hcnABC* operon) or *Eco*RI/*Hind*III restriction sites (*rhlA* and *wspF*). The gene replacement vectors were mobilized into *P. aeruginosa* via bi-parental conjugation, and the generation of the unmarked mutants was carried out as previously described (Pletzer *et al.*, 2014). The constructed gene knockout strains were verified by PCR amplification of the flanking region using the external primers followed by Sanger sequencing.

Quantitative real-time PCR

For RNA extraction, strains were grown for 24 h at 37°C in microtitre plates. Three wells were combined to form one sample. RNA was extracted using the RNeasy kit (Qiagen, Germany) followed by a DNase treatment (RQ1 DNase, Promega). A 500 ng aliquot of RNA was reverse transcribed using the ImProm-II reverse transcriptase (Promega). PCR reactions were performed using the SYBR Green Quantitect Kit (Qiagen, Germany) in duplicates. Primers are shown in Table S1. qPCRs were performed in a RotorGene 3000 (Corbett Research, Australia) using the following conditions: 2 min 95°C, followed by 35 cycles of 20 s at 95°C, 30 s at 60°C and 30 s at 72°C, followed by a final extension at 72°C for 3 min. To test for the presence of a unique PCR reaction product, melt curves were run after the amplification reaction. The *rpsL* gene was used as a reference housekeeping gene (Dumas *et al.*, 2006).

Acknowledgements

We are grateful to I. Schalk and G. Mislin (CNRS, University of Strasbourg, France) for the generous gift of pyochelin, pyoverdinin and protochelin. We thank P. François, W. Kelley, A. Renzoni and A. Luscher (University of Geneva) for providing *S. aureus* strains and for helpful discussions. This study was funded by grant No. 32473B-179289 from the Swiss National Science Foundation to CVD and supported by a grant to BGG from the Bertarelli Foundation (Geneva, Switzerland).

References

Abdel-Mawgoud, A.M., Aboulwafa, M.M., and Hassouna, N.A. (2009) Characterization of rhamnolipid produced by *Pseudomonas aeruginosa* isolate Bs20. *Appl Biochem Biotechnol* **157**: 329–345.

Abdel-Mawgoud, A.M., Lepine, F., and Deziel, E. (2010) Rhamnolipids: diversity of structures, microbial origins and roles. *Appl Microbiol Biotechnol* **86**: 1323–1336.

Adler, C., Corbalan, N.S., Seyedsayamdost, M.R., Pomares, M.F., de Cristobal, R.E., Clardy, J., *et al.* (2012) Catecholate siderophores protect bacteria from pyochelin toxicity. *PLoS One* **7**: e46754.

Allard, P.M., Peresse, T., Bisson, J., Gindro, K., Marcourt, L., Pham, V.C., *et al.* (2016) Integration of molecular networking and in-Silico MS/MS fragmentation for natural products dereplication. *Anal Chem* **88**: 3317–3323.

Bera, A., Biswas, R., Herbert, S., and Gotz, F. (2006) The presence of peptidoglycan O-acetyltransferase in various staphylococcal species correlates with lysozyme resistance and pathogenicity. *Infect Immun* **74**: 4598–4604.

Blanka, A., Duvel, J., Dotsch, A., Klinkert, B., Abraham, W. R., Kaever, V., *et al.* (2015) Constitutive production of c-di-GMP is associated with mutations in a variant of *Pseudomonas aeruginosa* with altered membrane composition. *Sci Signal* **8**: ra36.

Britigan, B.E., Roeder, T.L., Rasmussen, G.T., Shasby, D. M., McCormick, M.L., and Cox, C.D. (1992) Interaction of the *Pseudomonas aeruginosa* secretory products pyocyanin and pyochelin generates hydroxyl radical and causes synergistic damage to endothelial cells. Implications for *Pseudomonas*-associated tissue injury. *J Clin Invest* **90**: 2187–2196.

Calfee, M.W., Shelton, J.G., McCubrey, J.A., and Pesci, E. C. (2005) Solubility and bioactivity of the *Pseudomonas* quinolone signal are increased by a *Pseudomonas aeruginosa*-produced surfactant. *Infect Immun* **73**: 878–882.

Castric, K.F., and Castric, P.A. (1983) Method for rapid detection of cyanogenic bacteria. *Appl Environ Microbiol* **45**: 701–702.

Chambers, M.C., Maclean, B., Burke, R., Amodei, D., Ruderman, D.L., Neumann, S., *et al.* (2012) A cross-platform toolkit for mass spectrometry and proteomics. *Nat Biotechnol* **30**: 918–920.

Chua, S.L., Ding, Y., Liu, Y., Cai, Z., Zhou, J., Swarup, S., *et al.* (2016) Reactive oxygen species drive evolution of pro-biofilm variants in pathogens by modulating cyclic-di-GMP levels. *Open Biol* **6**: 160162.

Coffey, B.M., and Anderson, G.G. (2014) Biofilm formation in the 96-well microtiter plate. *Methods Mol Biol* **1149**: 631–641.

Coffman, T.J., Cox, C.D., Edeker, B.L., and Britigan, B.E. (1990) Possible role of bacterial siderophores in inflammation. Iron bound to the *Pseudomonas siderophore* pyochelin can function as a hydroxyl radical catalyst. *J Clin Invest* **86**: 1030–1037.

Cosson, P., Zulianello, L., Join-Lambert, O., Faurisson, F., Gebbie, L., Benghezal, M., *et al.* (2002) *Pseudomonas aeruginosa* virulence analyzed in a *Dictyostelium discoideum* host system. *J Bacteriol* **184**: 3027–3033.

D'Argenio, D.A., Calfee, M.W., Rainey, P.B., and Pesci, E.C. (2002) Autolysis and autoaggregation in *Pseudomonas aeruginosa* colony morphology mutants. *J Bacteriol* **184**: 6481–6489.

Drees, S.L., Ernst, S., Belviso, B.D., Jagmann, N., Hennecke, U., and Fetzner, S. (2018) PqsL uses reduced flavin to produce 2-hydroxylaminobenzoylacetate, a preferred PqsBC substrate in alkyl quinolone biosynthesis in *Pseudomonas aeruginosa*. *J Biol Chem* **293**: 9345–9357.

- Dumas, J.L., Van Delden, C., Perron, K., and Köhler, T. (2006) Analysis of antibiotic resistance gene expression in *Pseudomonas aeruginosa* by quantitative real-time-PCR. *FEMS Microbiol Lett* **254**: 217–225.
- Fletcher, M.P., Diggle, S.P., Camara, M., and Williams, P. (2007) Biosensor-based assays for PQS, HHQ and related 2-alkyl-4-quinolone quorum sensing signal molecules. *Nat Protoc* **2**: 1254–1262.
- Folkesson, A., Jelsbak, L., Yang, L., Johansen, H.K., Ciofu, O., Hoiby, N., et al. (2012) Adaptation of *Pseudomonas aeruginosa* to the cystic fibrosis airway: an evolutionary perspective. *Nat Rev Microbiol* **10**: 841–851.
- Frank, L.H., and Demoss, R.D. (1959) On the biosynthesis of pyocyanine. *J Bacteriol* **77**: 776–782.
- Garg, N., Wang, M., Hyde, E., da Silva, R.R., Melnik, A.V., Protsyuk, I., et al. (2017) Three-dimensional microbiome and metabolome cartography of a diseased human lung. *Cell Host Microbe* **22**: 705–716 e704.
- Gloag, E.S., Marshall, C.W., Snyder, D., Lewin, G.R., Harris, J.S., Santos-Lopez, A., et al. (2019) *Pseudomonas aeruginosa* interstrain dynamics and selection of hyperbiofilm mutants during a chronic infection. *MBio* **10**: e01698-19
- Goswami, D., Borah, S.N., Lahkar, J., Handique, P.J., and Deka, S. (2015) Antifungal properties of rhamnolipid produced by *Pseudomonas aeruginosa* DS9 against *Colletotrichum falcatum*. *J Basic Microbiol* **55**: 1265–1274.
- Guvener, Z.T., and Harwood, C.S. (2007) Subcellular location characteristics of the *Pseudomonas aeruginosa* GGDEF protein, WspR, indicate that it produces cyclic-di-GMP in response to growth on surfaces. *Mol Microbiol* **66**: 1459–1473.
- Haba, E., Pinazo, A., Jauregui, O., Espuny, M.J., Infante, M. R., and Manresa, A. (2003) Physicochemical characterization and antimicrobial properties of rhamnolipids produced by *Pseudomonas aeruginosa* 47T2 NCBIM 40044. *Bio-technol Bioeng* **81**: 316–322.
- Hickman, J.W., and Harwood, C.S. (2008) Identification of FleQ from *Pseudomonas aeruginosa* as a c-di-GMP-responsive transcription factor. *Mol Microbiol* **69**: 376–389.
- Hickman, J.W., Tifrea, D.F., and Harwood, C.S. (2005) A chemosensory system that regulates biofilm formation through modulation of cyclic diguanylate levels. *Proc Natl Acad Sci U S A* **102**: 14422–14427.
- Hoang, T.T., Karkhoff-Schweizer, R.R., Kutchma, A.J., and Schweizer, H.P. (1998) A broad-host-range Flp-FRT recombination system for site-specific excision of chromosomally-located DNA sequences: application for isolation of unmarked *Pseudomonas aeruginosa* mutants. *Gene* **212**: 77–86.
- Hoegy, F., Mislin, G.L., and Schalk, I.J. (2014) Pyoverdine and pyochelin measurements. *Methods Mol Biol* **1149**: 293–301.
- Hoffman, L.R., Deziel, E., D'Argenio, D.A., Lepine, F., Emerson, J., McNamara, S., et al. (2006) Selection for *Staphylococcus aureus* small-colony variants due to growth in the presence of *Pseudomonas aeruginosa*. *Proc Natl Acad Sci U S A* **103**: 19890–19895.
- Jensen, P.O., Bjarnshold, T., Phipps, R., Rasmussen, T.B., Calum, H., et al. (2007) Rapid necrotic killing of polymorphonuclear leukocytes is caused by quorum-sensing-controlled production of rhamnolipid by *Pseudomonas aeruginosa*. *Microbiology* **153**: 1329–1338.
- Kadurugamuwa, J.L., and Beveridge, T.J. (1996) Bacteriolytic effect of membrane vesicles from *Pseudomonas aeruginosa* on other bacteria including pathogens: conceptually new antibiotics. *J Bacteriol* **178**: 2767–2774.
- Kessler, E., Safrin, M., Abrams, W.R., Rosenbloom, J., and Ohman, D.E. (1997) Inhibitors and specificity of *Pseudomonas aeruginosa* LasA. *J Biol Chem* **272**: 9884–9889.
- Klosowska-Chomiczewska, I.E., Medrzycka, K., Hallmann, E., Karpenko, E., Pokynbroda, T., Macierzanka, A., et al. (2017) Rhamnolipid CMC prediction. *J Colloid Interface Sci* **488**: 10–19.
- Köhler, T., Kocjancic-Curty, L., Barja, F., Van Delden, C., and Pechère, J.C. (2000) Swarming of *Pseudomonas aeruginosa* is dependent on cell-to-cell signaling and requires flagella and pili. *J Bacteriol* **182**: 5990–5996.
- Köhler, T., Ouertatani-Sakouhi, H., Cosson, P., and van Delden, C. (2014) QsrO a novel regulator of quorum-sensing and virulence in *Pseudomonas aeruginosa*. *PLoS One* **9**: e87814.
- Kulasakara, H., Lee, V., Brencic, A., Liberati, N., Urbach, J., Miyata, S., et al. (2006) Analysis of *Pseudomonas aeruginosa* diguanylate cyclases and phosphodiesterases reveals a role for bis-(3'-5')-cyclic-GMP in virulence. *Proc Natl Acad Sci U S A* **103**: 2839–2844.
- Lepine, F., Milot, S., Deziel, E., He, J., and Rahme, L.G. (2004) Electrospray/mass spectrometric identification and analysis of 4-hydroxy-2-alkylquinolines (HAQs) produced by *Pseudomonas aeruginosa*. *J Am Soc Mass Spectrom* **15**: 862–869.
- Lightbown, J.W., and Jackson, F.L. (1954) Inhibition of cytochrome system of heart muscle and of *Staphylococcus aureus* by 2-heptyl-4-hydroxyquinoline-N-oxide, an antagonist of dihydrostreptomycin. *Biochem J* **58**: xlix.
- Limoli, D.H., and Hoffman, L.R. (2019) Help, hinder, hide and harm: what can we learn from the interactions between *Pseudomonas aeruginosa* and *Staphylococcus aureus* during respiratory infections? *Thorax* **74**: 684–692. <https://doi.org/10.1136/thoraxjnl-2018-212616>.
- Machan, Z.A., Taylor, G.W., Pitt, T.L., Cole, P.J., and Wilson, R. (1992) 2-Heptyl-4-hydroxyquinoline N-oxide, an antistaphylococcal agent produced by *Pseudomonas aeruginosa*. *J Antimicrob Chemother* **30**: 615–623.
- Marvig, R.L., Sommer, L.M., Molin, S., and Johansen, H.K. (2015) Convergent evolution and adaptation of *Pseudomonas aeruginosa* within patients with cystic fibrosis. *Nat Genet* **47**: 57–64.
- Mashburn-Warren, L., Howe, J., Garidel, P., Richter, W., Steiniger, F., Roessle, M., et al. (2008) Interaction of quorum signals with outer membrane lipids: insights into prokaryotic membrane vesicle formation. *Mol Microbiol* **69**: 491–502.
- Nguyen, A.T., Jones, J.W., Camara, M., Williams, P., Kane, M.A., and Oglesby-Sherrouse, A.G. (2016) Cystic fibrosis isolates of *Pseudomonas aeruginosa* retain iron-regulated antimicrobial activity against *Staphylococcus aureus* through the action of multiple Alkylquinolones. *Front Microbiol* **7**: 1171.
- Nitschke, M., Costa, S.G., and Contiero, J. (2010) Structure and applications of a rhamnolipid surfactant produced in soybean oil waste. *Appl Biochem Biotechnol* **160**: 2066–2074.

- Noordman, W.H., and Janssen, D.B. (2002) Rhamnolipid stimulates uptake of hydrophobic compounds by *Pseudomonas aeruginosa*. *Appl Environ Microbiol* **68**: 4502–4508.
- Nothias, L.F., Petras, D., Schmid, R., Dührkop, K., Rainer, J., Sarvepalli, A., et al. (2019) Feature-based molecular networking in the GNPS analysis environment. *bioRxiv*: 812404. <https://doi.org/10.1101/812404>.
- O'Connor, J.R., Kuwada, N.J., Huangyutitham, V., Wiggins, P.A., and Harwood, C.S. (2012) Surface sensing and lateral subcellular localization of WspA, the receptor in a chemosensory-like system leading to c-di-GMP production. *Mol Microbiol* **86**: 720–729.
- Ong, K.S., Cheow, Y.L., and Lee, S.M. (2017) The role of reactive oxygen species in the antimicrobial activity of pyochelin. *J Adv Res* **8**: 393–398.
- Pletzer, D., Lafon, C., Braun, Y., Köhler, T., Page, M.G., Mourez, M., et al. (2014) High-throughput screening of dipeptide utilization mediated by the ABC transporter DppBCDF and its substrate-binding proteins DppA1–A5 in *Pseudomonas aeruginosa*. *PLoS ONE* **9**: e111311.
- Pluskal, T., Castillo, S., Villar-Briones, A., and Oresic, M. (2010) MZmine 2: modular framework for processing, visualizing, and analyzing mass spectrometry-based molecular profile data. *BMC Bioinformatics* **11**: 395.
- Radlinski, L., Rowe, S.E., Kartchner, L.B., Maile, R., Cairns, B.A., Vitko, N.P., et al. (2017) *Pseudomonas aeruginosa* exoproducts determine antibiotic efficacy against *Staphylococcus aureus*. *PLoS Biol* **15**: e2003981.
- Rudin, L., Sjöstrom, J.E., Lindberg, M., and Philipson, L. (1974) Factors affecting competence for transformation in *Staphylococcus aureus*. *J Bacteriol* **118**: 155–164.
- Rutz, A., Dounoue-Kubo, M., Ollivier, S., Bisson, J., Bagheri, M., Saesong, T., et al. (2019) Taxonomically informed scoring enhances confidence in natural products annotation. *Front Plant Sci* **10**: 1329.
- Samadi, N., Abadian, N., Ahmadvani, R., Amini, F., Dalili, D., Rastkari, N., et al. (2012) Structural characterization and surface activities of biogenic rhamnolipid surfactants from *Pseudomonas aeruginosa* isolate MN1 and synergistic effects against methicillin-resistant *Staphylococcus aureus*. *Folia Microbiol (Praha)* **57**: 501–508.
- Smith, E.E., Buckley, D.G., Wu, Z., Saenphimmachak, C., Hoffman, L.R., D'Argenio, D.A., et al. (2006) Genetic adaptation by *Pseudomonas aeruginosa* to the airways of cystic fibrosis patients. *Proc Natl Acad Sci U S A* **103**: 8487–8492.
- Soberon-Chavez, G., Lepine, F., and Deziel, E. (2005) Production of rhamnolipids by *Pseudomonas aeruginosa*. *Appl Microbiol Biotechnol* **68**: 718–725.
- Song, F., Wang, H., Sauer, K., and Ren, D. (2018) Cyclic-di-GMP and oprF are involved in the response of *Pseudomonas aeruginosa* to substrate material stiffness during attachment on polydimethylsiloxane (PDMS). *Front Microbiol* **9**: 110.
- Spiers, A.J., Kahn, S.G., Bohannon, J., Travisano, M., and Rainey, P.B. (2002) Adaptive divergence in experimental populations of *Pseudomonas fluorescens*. I. Genetic and phenotypic bases of wrinkly spreader fitness. *Genetics* **161**: 33–46.
- Starkey, M., Hickman, J.H., Ma, L., Zhang, N., De Long, S., Hinz, A., et al. (2009) *Pseudomonas aeruginosa* rugose small-colony variants have adaptations that likely promote persistence in the cystic fibrosis lung. *J Bacteriol* **191**: 3492–3503.
- Szamosvari, D., and Bottcher, T. (2017) An unsaturated quinolone N-oxide of *Pseudomonas aeruginosa* modulates growth and virulence of *Staphylococcus aureus*. *Angew Chem Int Ed Engl* **56**: 7271–7275.
- Tognon, M., Kohler, T., Gdaniec, B.G., Hao, Y., Lam, J.S., Beaume, M., et al. (2017) Co-evolution with *Staphylococcus aureus* leads to lipopolysaccharide alterations in *Pseudomonas aeruginosa*. *ISME J* **11**: 2233–2243. <https://doi.org/10.1038/ismej.2017.83>.
- Valentini, M., and Filloux, A. (2016) Biofilms and cyclic di-GMP (c-di-GMP) signaling: lessons from *Pseudomonas aeruginosa* and other bacteria. *J Biol Chem* **291**: 12547–12555.
- Voggu, L., Schlag, S., Biswas, R., Rosenstein, R., Rausch, C., and Gotz, F. (2006) Microevolution of cytochrome bd oxidase in staphylococci and its implication in resistance to respiratory toxins released by pseudomonas. *J Bacteriol* **188**: 8079–8086.
- Wang, M., Carver, J.J., Phelan, V.V., Sanchez, L.M., Garg, N., Peng, Y., et al. (2016) Sharing and community curation of mass spectrometry data with global natural products social molecular networking. *Nat Biotechnol* **34**: 828–837.
- Winson, M.K., Swift, S., Fish, L., Throup, J.P., Jorgensen, F., Chhabra, S.R., et al. (1998) Construction and analysis of luxCDABE-based plasmid sensors for investigating N-acyl homoserine lactone-mediated quorum sensing. *FEMS Microbiol Lett* **163**: 185–192.
- Wittgens, A., Tiso, T., Arndt, T.T., Wenk, P., Hemmerich, J., Muller, C., et al. (2011) Growth independent rhamnolipid production from glucose using the non-pathogenic *Pseudomonas putida* KT2440. *Microb Cell Fact* **10**: 80.
- Zulianello, L., Canard, C., Köhler, T., Caille, D., Lacroix, J.S., and Meda, P. (2006) Rhamnolipids are virulence factors that promote early infiltration of primary human airway epithelia by *Pseudomonas aeruginosa*. *Infect Immun* **74**: 3134–3147.

Supporting Information

Additional Supporting Information may be found in the online version of this article at the publisher's web-site:

Figure S1. Supporting information.

Table S1. Strains, plasmids and primers used in this study.